AN INVESTIGATION ON VERTICAL TAILPLANE DESIGN

Fabrizio Nicolosi

Dep. of Aerospace Engineering

University of Naples

Federico II

Via Claudio, 21

80125 Napoli - Italy

fabrnico@unina.it

Pierluigi Della Vecchia

Dep. of Aerospace Engineering

University of Naples

Federico II

Via Claudio, 21

80125 Napoli - Italy

pierluigi.dellavecchi

a@unina.it

Danilo Ciliberti

Dep. of Aerospace Engineering

University of Naples

Federico II

Via Claudio, 21

80125 Napoli - Italy

dancili@gmail.com

Abstract. The paper presents an attempt to compare some methods and to propose guidelines for the preliminary design of the vertical tailplane (through correct estimation of its contribution and efficiency) in particular for regional turboprop and commuter aircraft configurations. In the first part, the paper deals with the analysis of the existing semi‑empirical methodologies used in preliminary design phase to estimate the contribution of vertical tailplane on aircraft directional stability and control. The classical method proposed by Roskam (taken basically from USAF DATCOM) and the method reported in ESDU reports have been carefully analyzed in details. Both derive from NACA reports of the first half of the '900, based on obsolete geometries, and give quite different results for certain configurations, e. g. in the case of horizontal stabilizer mounted in fuselage. In a second phase several CFD (Navier-Stokes, N‑S) calculations have been performed on some test cases (used as experimental database) described in NACA reports and used in the past to obtain the semi‑empirical methodology reported in USAF DATCOM, to verify the compliance of CFD results with available experimental data. The CFD calculations (performed through the use of a parallel supercomputing platform) have shown a good agreement between numerical and experimental data. A large number of simulations were run in the SCoPE grid infrastructure of the University of Naples Federico II that gave the possibility to simulate complex 3D geometries in a small amount of time. Subsequently a new set of aircraft configurations, typical of propeller engine transport aircraft, and in particular typical of regional turboprop, have been created and prepared for CFD analysis. The different configurations that have been prepared differs for wing aspect ratio, wing‑fuselage relative position (high‑wing/low‑wing), vertical tailplane aspect ratio (vertical tail span versus fuselage radius) and horizontal tailplane position respect to the vertical tailplane (in particular investigation the effect of fin‑mounted T configuration, typical of regional turboprop transport aircraft). For all configurations the computational mesh has been carefully analyzed and prepared. All the CFD N‑S analyses will be useful to obtain new semi‑empirical curves to predict the above-mentioned effect and to have a correct and more accurate estimation of vertical tailplane contribution to aircraft directional stability and control. The final aim, through the performed CFD calculations, is to present some new guidelines and a new method to be applied for the correct design of vertical tailplane, in particular for transport regional turboprop and commuter aircraft.

Keywords. Vertical tailplane aerodynamics, directional stability, aircraft preliminary design

1 Introduction

Tailplane design needs an accurate determination of stability derivatives. The more accurate the latter the better the former. Nowadays the most known semi-empirical methods that estimate these derivatives are the USAF DATCOM [4], proposed by Roskam [9], and the ESDU [5] methods. These are mainly based on NACA reports from the '30s to the '50s, contemplating obsolete geometries as elliptical bodies, swept wings and short fuselages (Figure 1), in contrast with the shape of the actual props airliners; moreover they present big discrepancies for certain configuration such as the horizontal tailplane mounted in fuselage. Both of them start from the definition of the isolated vertical tailplane lift curve slope $C_{L\alpha v}$ and modify it by means of corrective factors to obtain the final sideforce due to sideslip derivative $C_{Y\beta v}$. These semi-empirical factors provide for the effects of the fuselage, wing and horizontal tailplane on the vertical tailplane. Stability derivative $C_{N\beta v}$ and rolling moment derivative $C_{\mathcal{L}\beta v}$ are function of $C_{Y\beta v}$ tail position and angle of attack.
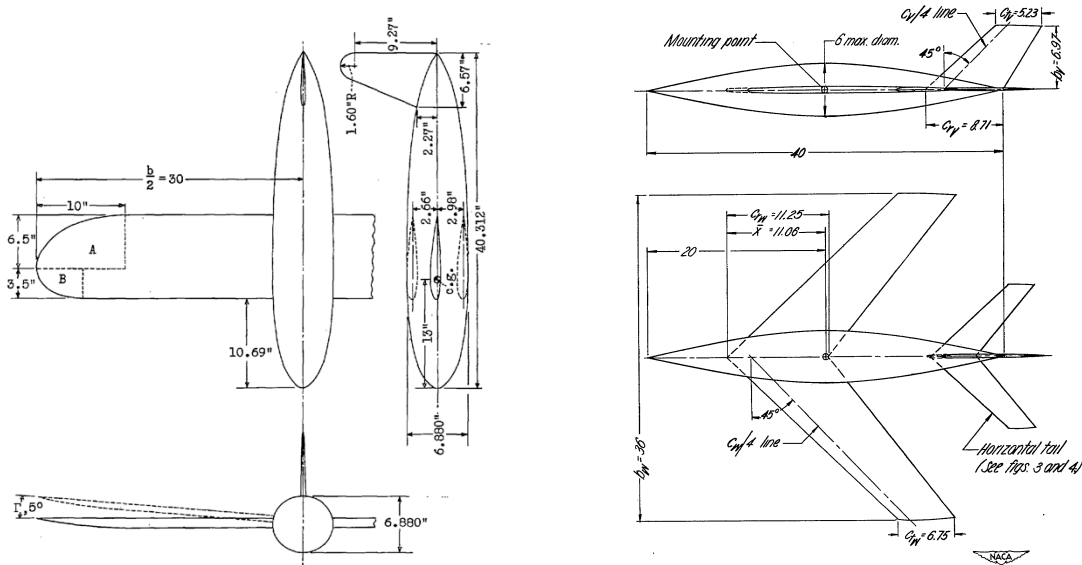

Figure 1: Some of the geometries used in NACA reports.

According to USAF DATCOM [4], resumed by Roskam [9], the sideslip derivative $C_{Y\beta v}$ is made up of three components: body cross-flow, horizontal surface, wing-body wake and sidewash effect (the latter two lumped into a single effectiveness parameter). The first two define an *effective* vertical tail aspect ratio to be substituted in the $C_{L\alpha v}$ formula instead of the geometric aspect ratio then the lift gradient is corrected again by the sidewash effect and other semi-empirical factors.

The procedure proposed by ESDU [5] is quite simple: the sideslip derivative $C_{Y\beta v}$ is obtained by multiplying the vertical tail lift curve slope $C_{L\alpha v}$ by three semi-empirical factors that account for the effect of the fuselage, wing and horizontal tailplane. However, there's no wing wake effect, the sidewash is considered constant; moreover the geometric aspect ratio is differently defined.

Modern approaches make use of CFD, from panel methods to RANS. At DIAS (Department of Aerospace Engineering of the University of Naples Federico II), the former are used in an internally developed code, a software that allows the calculation of the nonlinear aerodynamic characteristics of arbitrary configurations in subsonic flow. Potential flow is analyzed with a subsonic panel method; the program is a surface singularity distribution based on Green's identity. Nonlinear effects of wake shape are treated in an iterative wake relaxation procedure; the effects of viscosity are treated in an iterative loop coupling potential flow and integral boundary layer calculations. The compressibility correction is based on Prandtl-Glauert rule [6].

The RANS approach is currently being investigated at DIAS, with the commercial CFD software Star-CCM+. More details will follow in Section 1.2.

1.1 Comparing semi-empirical methods

To compare the semi-empirical methods described above, a MATLAB program has been written. Given an aircraft configuration, the script permits parametric studies as well as one shot runs. Actually it is possible to investigate the subsequent parameters:

- Geometric tail aspect ratio;
- Wing fuselage relative position;
- Wing aspect ratio;
- Wing span;
- Horizontal tailplane relative position;
- Horizontal tailplane size;
- Vertical tail span vs. fuselage depth (thickness);
- Fuselage upsweep angle.

Given the ATR-42 aircraft, Figure 2 show the effect of changing the ratio between vertical tail span and fuselage thickness (left) and the horizontal tailplane position on the vertical tailplane (right). It is apparent that semi-empirical methods become less reliable for those configurations with very different results.
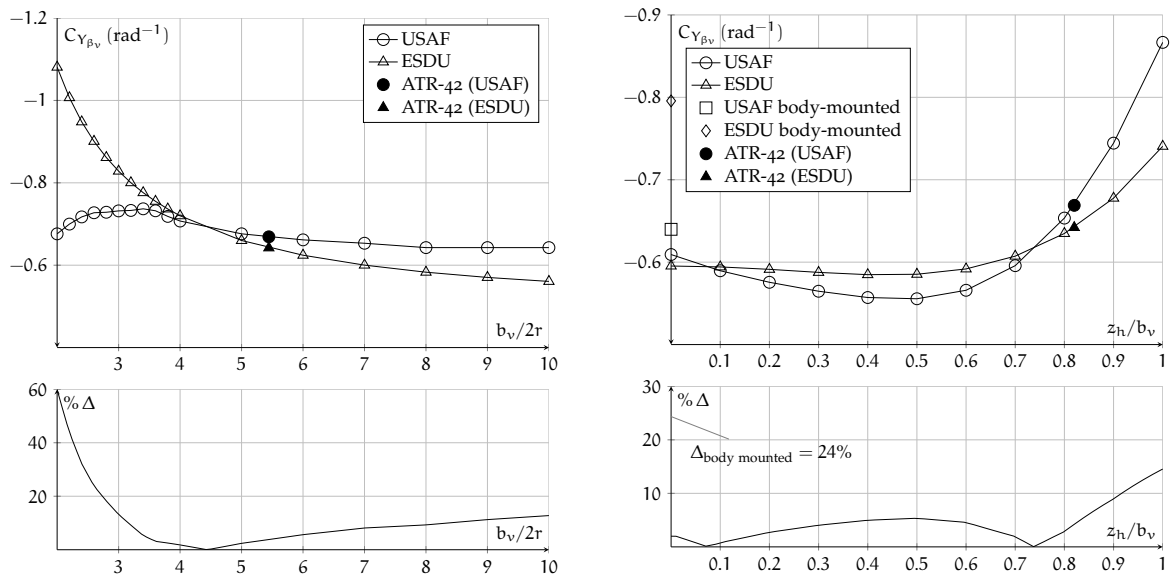

Figure 2: Effect of change the vertical tail span to fuselage thickness (left) and the horizontal tail position on vertical tail (right) on the vertical tail sideforce derivative.

1.2 The CFD approach

The new approach adopted at the DIAS consists in the use of the commercial CFD software StarCCM+. This software permits to work in an integrated environment, where it is possible to import (or generate, if the model is very simple) the CAD geometry, automatically generate a mesh, easily setup the physics, run the analysis and visualize the results as plots and scenes. One of its interesting features is the polyhedral cells mesh type: every cell is a polyhedral with an average of 14 faces. This permits a less number of cells in a numerical domain, thus saving memory used per CPU.

StarCCM+ was often used on the University's grid computing infrastructure (SCoPE) to simulate lots of configurations in a short amount of time. 128 licenses (one per CPU) were available for this investigation. Figure 3 on the left shows that doubling the CPUs number the time to convergence halves, while on the right shows some pictures of the fiber optics cables of SCoPE.
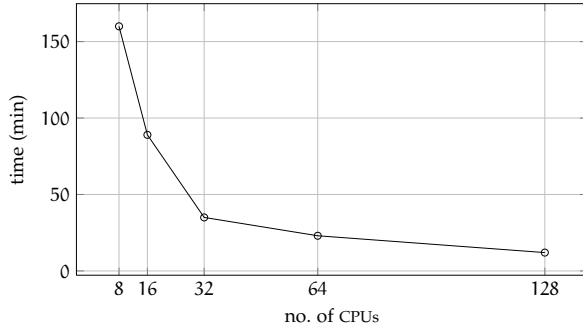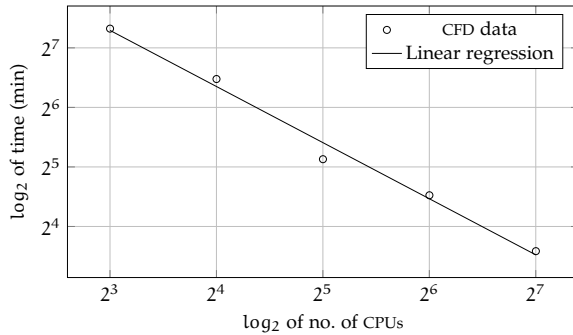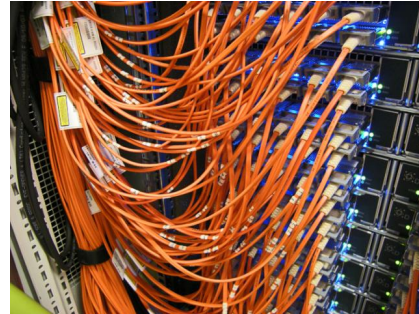

(a) *Linear plot.*

(a) *Three rack servers of the data center.*

(b) *Logarithmic plot.*

(c) *Fiber optic connections.*

Figure 3: Time vs. CPUs number (left) and the SCoPE grid infrastructure (right).

2 NACA test cases with StarCCM+

In order to check the compliance of the CFD results with available test data, three test cases have been performed. These are a longitudinal test case and two directional test cases.

2.1 NACA report 540

In the work of Eastmen and Kenneth [3] 209 wing-fuselage combinations were tested in the NACA variable-density wind tunnel, to provide information about the effects of aerodynamic interference between wings and fuselage at a large value of the Reynolds number (3100000). The wing section is a NACA 0012 airfoil. Three of these combinations (respectively mid, high and low wing, marked no. 7, 22 and 67 in ref. [3]) plus a wing-alone configuration were chosen for the test case. In short, for each combination, a round fuselage with a rectangular wing has been analyzed at various angles of incidence, in symmetric flow. No discussion is made on the results since the primary interest of this section is the check of the previously stated compliance.

Results in terms of the aerodynamic lift, effective profile drag and moment coefficient C_L, C_{De} and C_M are shown, for the mid-wing combination, in Figure 4. Effective profile drag coefficient is defined as the difference between the total drag coefficient C_D and the minimum induced drag coefficient C_{Di} that is

$$C_{De} = \frac{C_D - C_L^2}{\pi A}$$

and this to account only for induced drag due to the interference of the wing-body combination.

From the charts (only the mid-wing combination is shown) it is apparent the validity of the mesh and of the physics model involved (Spalart-Allmaras turbulence model), as the configurations at small angle of attack are well simulated by the CFD.
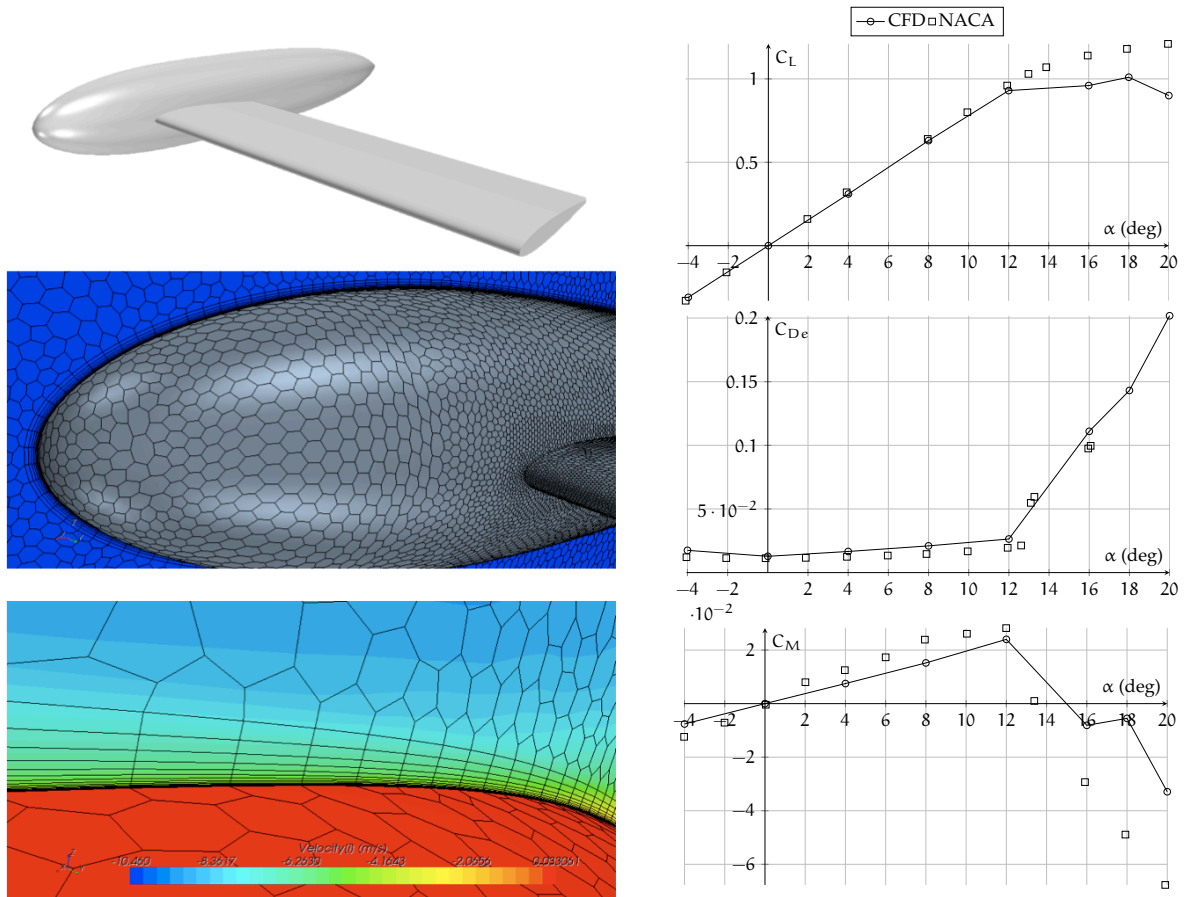

Figure 4: Results for the NACA report 540 (mid-wing combination).

2.2 NACA report 730

In the report of Bamber and House [1], a NACA 23012 rectangular wing with rounded tips was tested with a round fuselage at several angles of sideslip, in a high, mid and low wing combination. Moreover each combination was tested with and without fin. The fin was made to the NACA 0009 section with an area of 45 sq. in. No dihedral angle and no flap device were considered. Reynolds number is 609000 based on wing chord. Results are evaluated in terms of the rolling moment, yawing moment and sideforce due to sideslip coefficients (for the whole configuration) $C_{\mathcal{L}\beta}$, $C_{N\beta}$ and $C_{Y\beta}$. All derivatives are per deg and evaluated assuming linearity with β between 0° and 5°. The chart shown in Figure 5 is for the wing-body fin configuration.
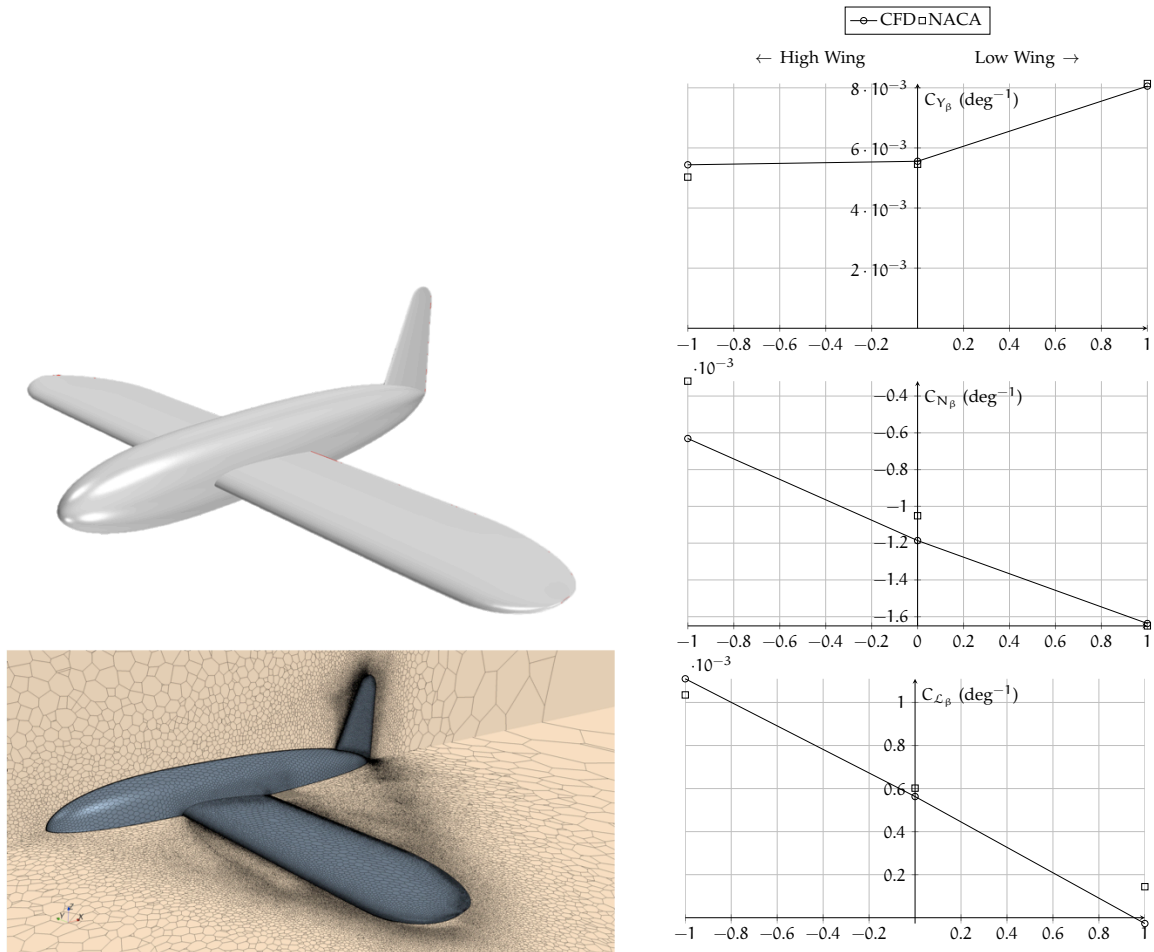
Figure 5: Results for the NACA report 730 (wing-body-fin combination).

2.3 NACA report 1049

The aim of the work of Queijo and Wolhart [8] was to investigate the effects of vertical tail size and span and of fuselage shape and length on the static lateral stability characteristics of a model with 45° swept back (quarter chord line) wing and vertical tail, NACA 65A008 airfoil. In this report is highlighted an interesting relation between the effective aspect ratio of the vertical tail and the fuselage thickness where the tail is located and this was resumed by the USAF DATCOM method. For the purpose of the test case, only a combination with a round fuselage was simulated. Results are shown in Figure 6 in terms of force and moment coefficients.

In conclusion, the results obtained with the CFD are close enough to the experimental results, so it appeared reasonable to use Star-CCM+ for the investigation on vertical tailplane design discussed in the next section.
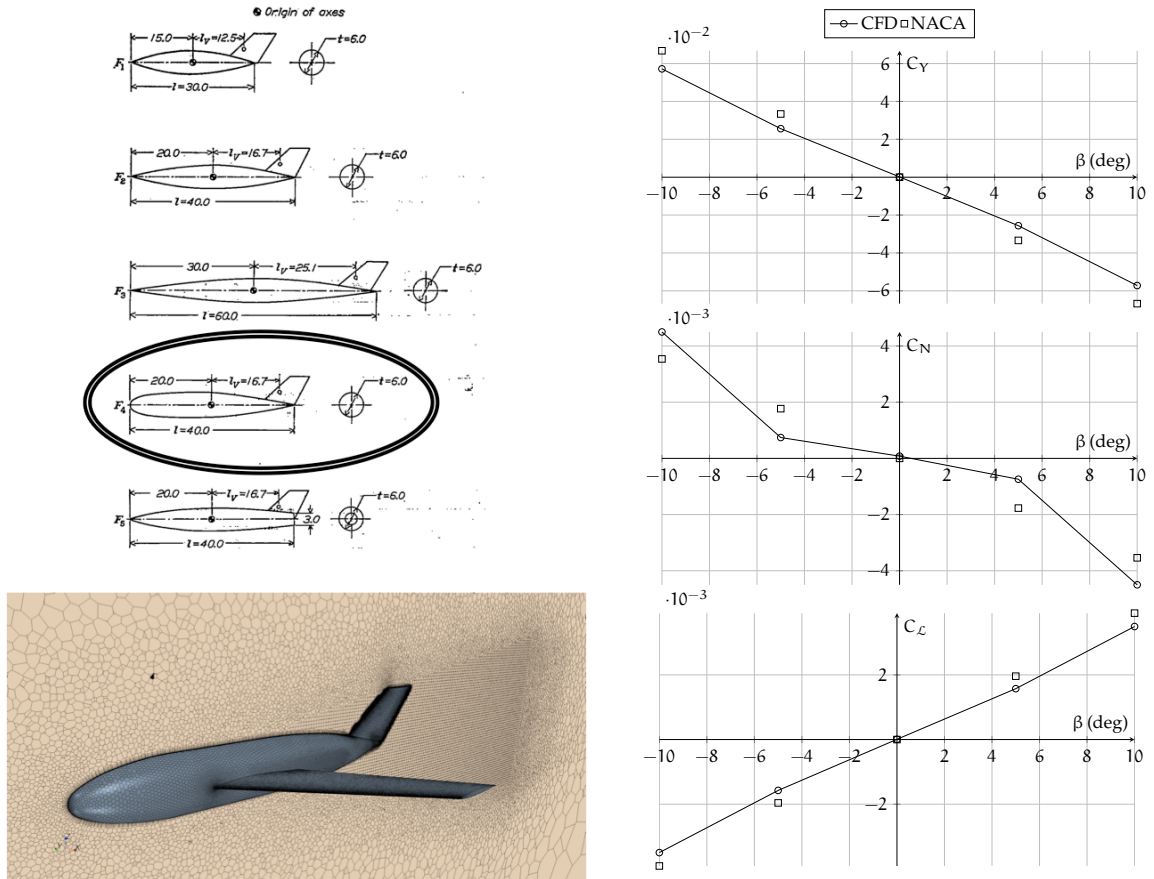
Figure 6: Results for the NACA report 1049 (wing-body-fin combination).

3   A new investigation

The CFD investigation on aircraft components' interference on sideforce derivative is carried on a typical turboprop geometry, synthesis of the ATR-72 and NGTP-5 airplanes.
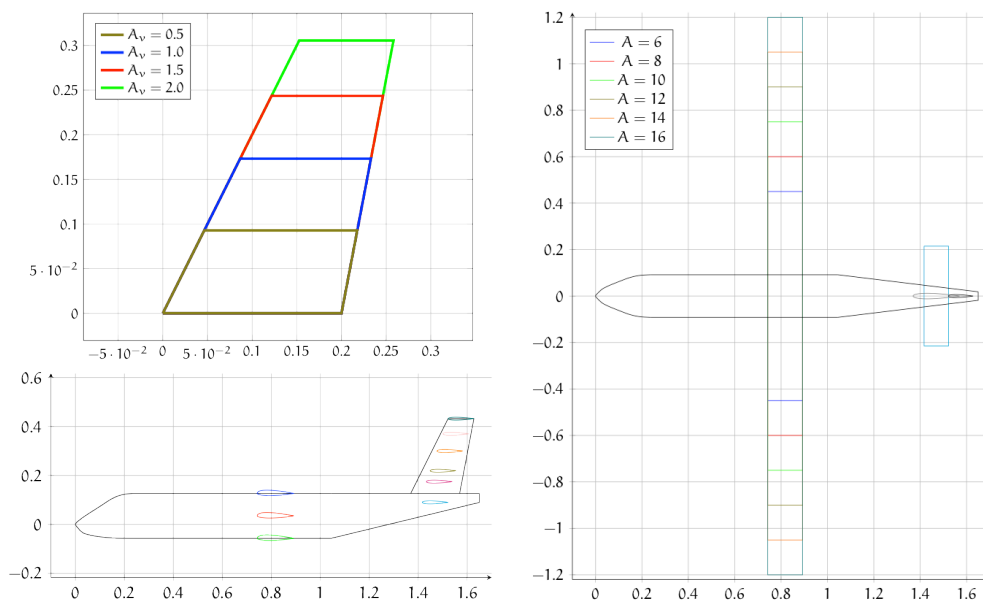

Figure 7: Geometries of the CFD model.

	fuselage slenderness l_f/d_f	nose ratio l_n/l_f	cone ratio l_c/l_f	wing position $x_{w_{LE}}/l_f$
	Fuselage parameters			
ATR-72	10.3	1.3	3.2	0.41
NGTP-5	9	1.3	3.3	0.47
CFD model	9	1.3	3.3	0.45

	A_v	λ_v	$\Lambda_{v_{LE}}$	$\Lambda_{v_{TE}}$	S_v/S	$x_{v_{LE}}/l_f$	$\bar{V}_v$
	Vertical tail parameters						
ATR-72	1.56	0.61	32°	17°	0.20	0.83	0.098
NGTP-5	1.43	0.63	29°	15°	0.24	0.85	0.110
CFD model	variable	variable	30°	15°	variable	variable	variable

	A_h	λ_h	$\Lambda_{h_{LE}}$	$\Lambda_{h_{TE}}$	S_h/S	$x_{h_{LE}}/l_f$	$\bar{V}_h$
	Horizontal tail parameters						
ATR-72	4.1	n. a.	n. a.	n. a.	0.18	n. a.	0.19
NGTP-5	4.1	n. a.	n. a.	n. a.	0.25	n. a.	0.19
CFD model	4.1	0	0°	0°	0.20	variable	variable

Table 1: Characteristics of the model to be investigated by CFD.

3.1 Preliminary studies

Before to attempt any analysis, it was necessary to perform some preliminary tests to define the correct mesh and physics parameters: base size and Reynolds number. The base size is a reference length to which the size of all cells is related. It permits to scale the whole mesh by varying a single parameter. Given the aircraft configuration shown in Figure 8, the most complicated mesh due to the intersections among components, the left part of the figure shows that the optimum base size is 1.65 m, corresponding to about 10 millions of polyhedral cells for that configuration. Once chosen the base size the study on Reynolds number has been performed. In the lower right part of the same figure it is shown the insensitivity to the Reynolds number up to an angle of sideslip of 10°. The turbulence model chosen is Spalart-Allmaras. These results permit to define the sideforce derivative as the ratio of C_v evaluated at $\beta = 5°$

$$C_{Y\beta v} \approx \frac{C_{Yv}(5°) - 0}{5° - 0°} = \frac{C_{Yv}(5°)}{5} \ \text{deg}^{-1}$$
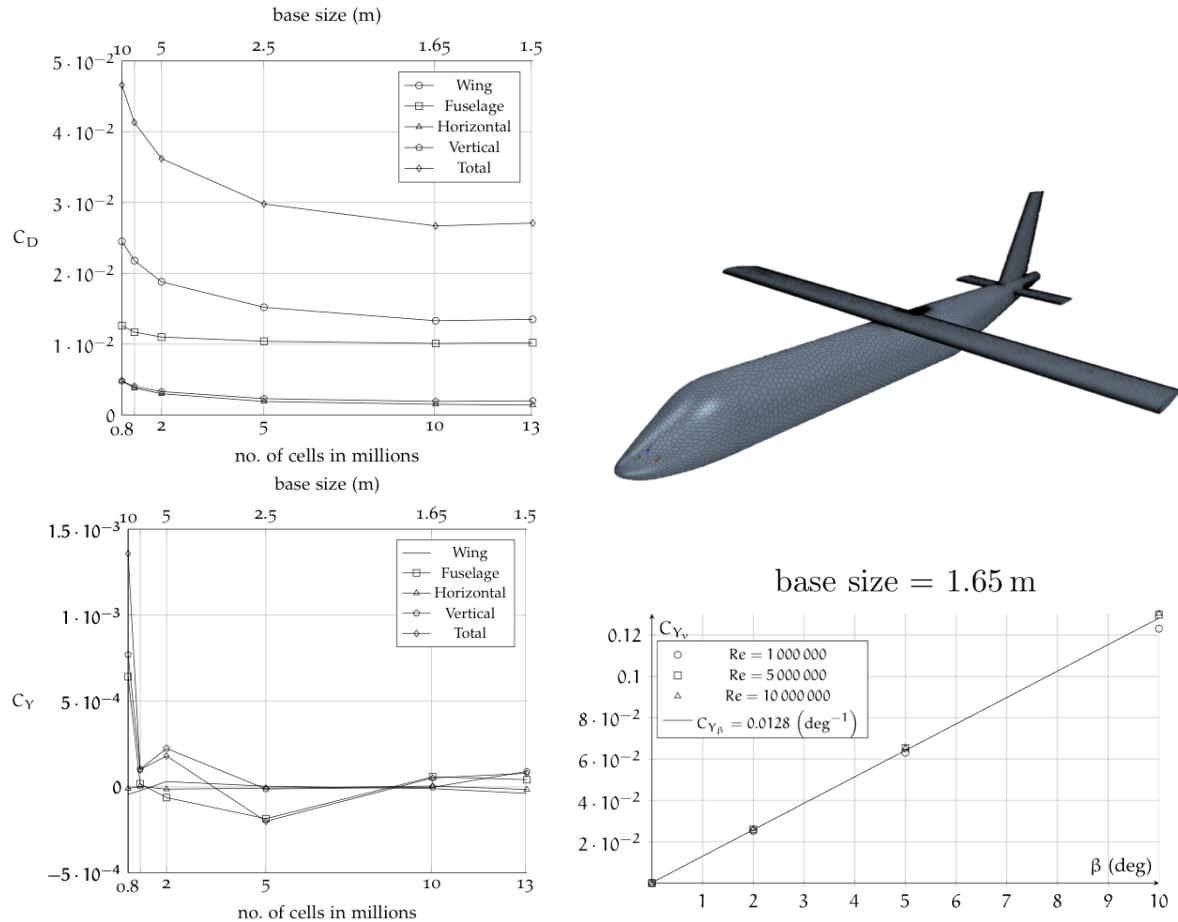
Figure 8: Results of the preliminary tests: variation of the aerodynamic coefficients with base size (left) and insensitivity to Reynolds number (lower right) for the configuration depicted on upper right.

3.2 CFD analyses

Having frozen mesh and physics parameter CFD analyses were performed on several configuration, from the isolated vertical tailplane to the complete aircraft. The effect of each component on the vertical tail was evaluated by means of ratios of $C_{Y\beta v}$ between configurations, to highlight the interference. For example, the effect of adding the fuselage to the isolated vertical tail was obtained by dividing the $C_{Y\beta v}$ of the body-vertical configuration by the $C_{Y\beta v}$ of the isolated vertical tail (with the same aspect ratio, planform and mesh parameters).

Almost all analyses, except for the smaller simulation files, were solved on the SCoPE grid infrastructure. The polyhedral mesh and the Spalart-Allmaras turbulence models were chosen to solve the asymmetrical flow field. All of the runs were solved in incompressible flow, Re = 1000000, at α = 0° and β = 5°, since the angle of attack is not relevant for directional stability and with a sideslip of 5° the effects are linear, that is the aircraft is in cruise condition. The mesh parameters, common to all analyses, are reported in Table 2.

Mesh type	polyhedral cells		
Base size	1.65 m		
Number of prism layers	20		
Prism layer stretching	1.1		
Block shape size	$60 \times 30 \times 20\,\mathrm{m}^3$		
Mesh size (in percentage of the base size)			
	Minimum	Target	Prism layer
Wing	0.04	0.5	0.02
Fuselage	0.1	1.0	0.02
Horizontal	0.04	0.5	0.02
Vertical	0.05	0.5	0.01
Angle of attack α	0°		
Angle of sideslip β	5°		
Reynolds number Re	1 000 000 (based on wing chord)		
Mach number M	0		
Flow regime	fully turbulent (Spalart-Allmaras model)		

Table 2: Mesh and physics data common to all CFD analyses.

3.2.1 Isolated vertical tail

The vertical tail alone has to be analyzed for three reasons: CFD results must verify linearity be compatible with theory and provide the lift gradient $C_{L\alpha v}$. Beyond the vertical tailplane of the CFD model, represented in Figure 7, a rectangular and a constant taper ratio tailplanes were analyzed (Figure 9). Here it is noted that the CFD model component has a constant sweep angle, but a variable taper ratio, and the behavior predicted by CFD is the same of that predicted by the curves reported in literature, as shown in Figure 10. The rectangular tailplane has only a slightly higher trend respect to the swept one and this is in contrast with theory that provides a much higher lift gradient. The constant taper vertical tailplane does not agree with theory simply because it has variable sweep with aspect ratio and hence it should not be compared at all.
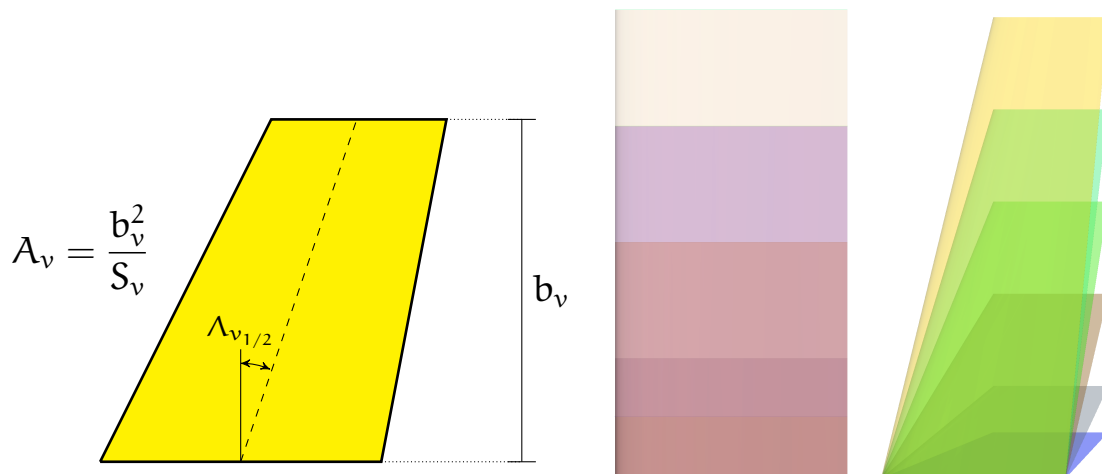

Figure 9: Definition of the parameters of the isolated vertical tail (left). Sequences of straight (center) and constant tapered (right) vertical tailplanes analyzed.
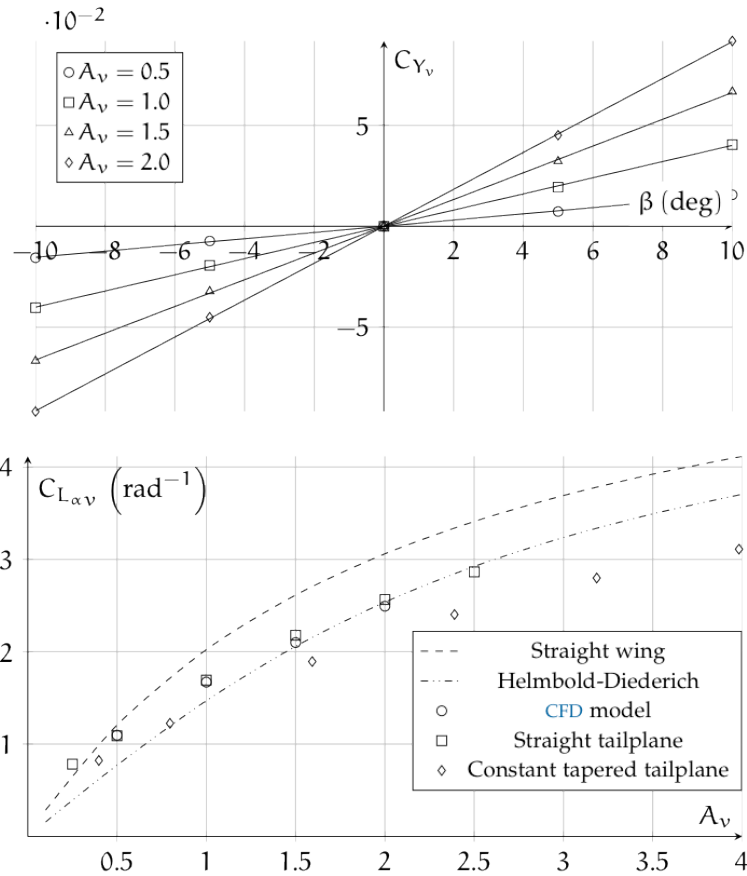
Figure 10: Linearity (up) and compliance with theory (down) for the isolated vertical tails.

3.2.2 Fuselage effect

The first coupling effect studied was that of fuselage. This effect is measured by the ratio between the sideforce coefficients of the body-vertical configurations of Figure 11 left and those of the isolated vertical tails previously analyzed.

Theory [10] and experiment [4, 5] suggest that the fuselage acts as a cylinder at the wing-tip, accelerating the flow and increasing the sideforce on the vertical tail.

Results, in terms of the C_{Y_v} ratios vs $b_v/2r$, are shown in Figure 11 right. Here b_v is the geometric tail span of the isolated vertical tail, not the one defined by Roskam [9], that is there's no tail span extension to the fuselage centerline. The parameter $2r$ is again the fuselage thickness on the x location of the aerodynamic center of the vertical tailplane. It can be seen a little scatter among different tailplanes of different aspect ratios, sweep angles and taper ratios, even at low $b_v/2r$ ratios (i.e. little tailplanes on a big fuselage), instead of the results of Queijo and Wolhart [8] reported in Figure 13, where there's a bigger data scatter, especially among tails of different aspect ratio.
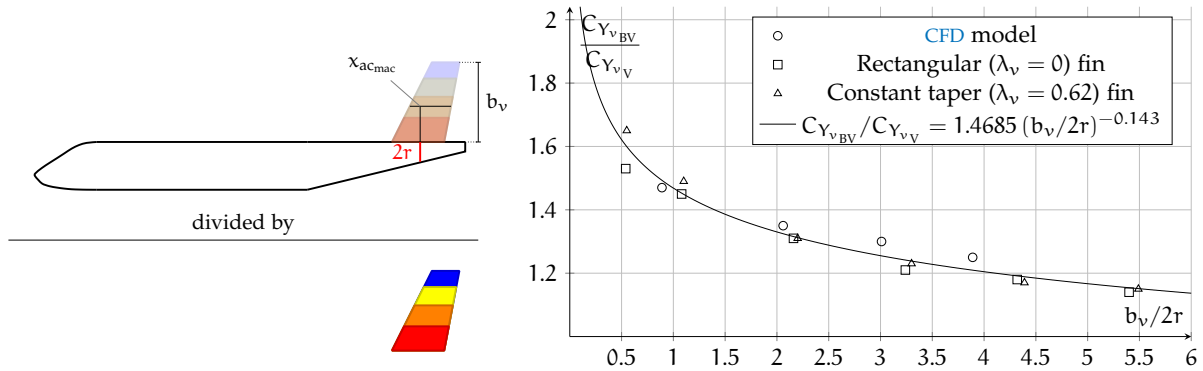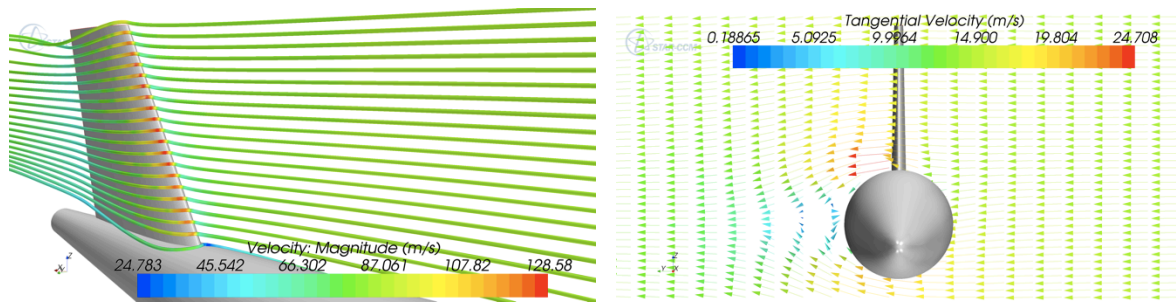
Figure 11: Body effect.

Figure 12: Streamlines (left) and tangential velocity vectors (right) on a transversal section of the vertical tail.
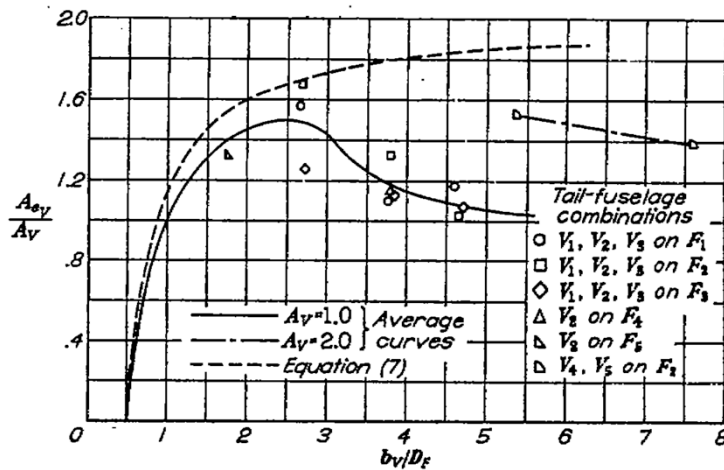

Figure 13: The body effect according to NACA report 1049 [8].

3.2.3 Wing effect

The objective of these analyses is the evaluation of the effect of wing position and aspect ratio on the sideforce of the vertical tail. In order to achieve this, several rectangular wings, of different aspect ratio, were simulated at high, mid and low position in fuselage. Combinations involved are depicted in Figure 14, while results are shown – in terms C_{Yv} ratios between configurations – in Figure 15. The choice of the vertical tailplanes aspect ratios' $A_v = 1$ and $A_v = 2$ is due to consider two extreme values of this parameter: since the scatter between these values is negligible, it can be argued that the effect of the wing on the C_{Yv} is independent from the choice of the vertical tailplane.

For high wing Figure 15a shows that C_{Yv} decreases with wing aspect ratio A of about 5%, with respect to the body-vertical configuration.

Mid wing has no effect; it is neutral from a directional point of view, as reported by Perkins and Hage [7]. Data spread (Figure 15b) is negligible, around 1% of unity.

For low wing the C_{Y_v} decreases with wing aspect ratio A, probably because of the decreasing magnitude of tip vortices with aspect ratio. In this configuration, however, there's an increase of about 5% of the sideforce coefficient (Figure 15c), with respect to the body-vertical configuration.
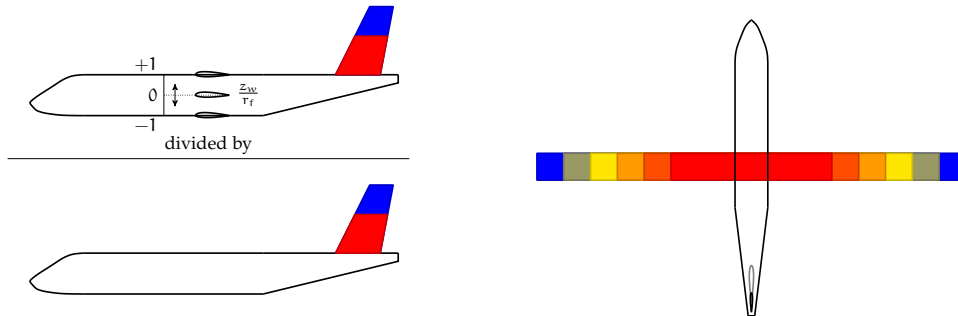

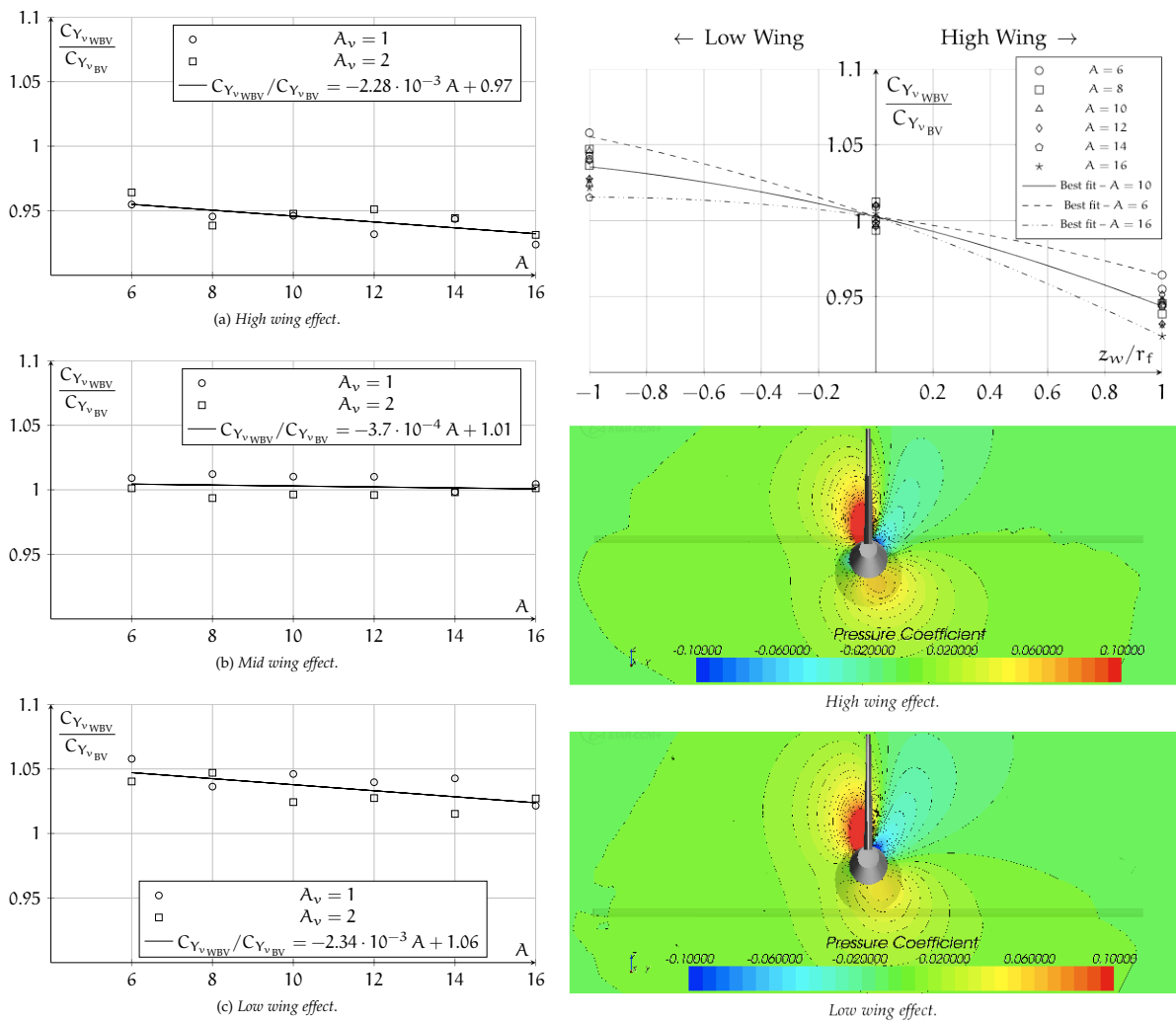Figure 14: Configurations involved in the analyses of wing effect.

Figure 15: Wing effect.

3.2.4 Horizontal tailplane effect

The horizontal tailplane influences the vertical tailplane with its position and size. The former is a major effect, while the latter has a minor influence, especially for tailplanes of the same surface.

A straight horizontal tailplane, of constant size and aspect ratio (Figure 16, Table 1), is mounted in five positions on the fin and one on the fuselage. Then, the same horizontal tailplane, initially centered in chord, is moved forward and rearward by 25% of the local vertical tailplane chord.

Results are shown in Figure 17 left, in terms of C_{Y_v} ratios between the wing-body-fin-horizontal configuration (i.e. the complete airplane) and the wing-body-fin configuration. The trend is much similar to that of Figure 18 by Brewer and Lichtenstein [2], that is the effect of positioning the horizontal tailplane on the fuselage and on the free tip of the vertical tailplane is almost the same. It is apparent that the screening effect of the horizontal tailplane is maximum at extreme positions and decreases moving it forward.

The effect of tailplanes' relative size is shown in Figure 17 right, where it is represented the ratio C_{Y_v} between the complete airplane with the horizontal tail varying in size and the previous configuration with a ratio S_h/S_v close to unity (the original horizontal tailplane). Two extreme positions were analyzed, that is the body-mounted and tip-mounted.

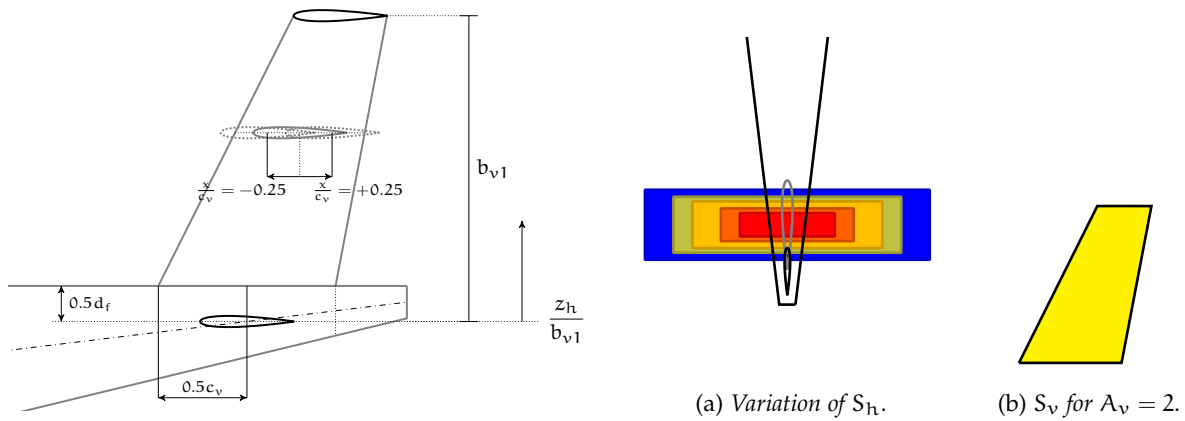(a) *Variation of* S_h.   (b) S_v *for* $A_v = 2$.

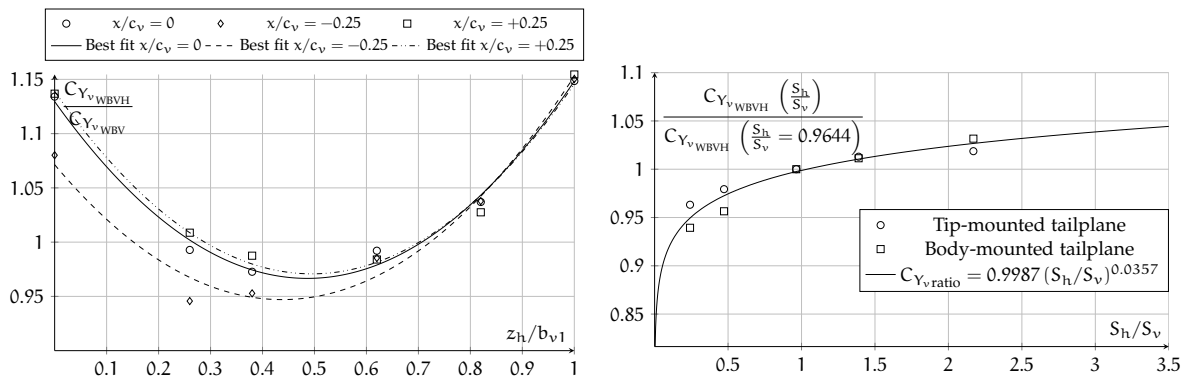Figure 16: Configurations involved in the analyses on the horizontal tailplane effect.

Figure 17: Effect of horizontal tailplane position (left) and size (right)
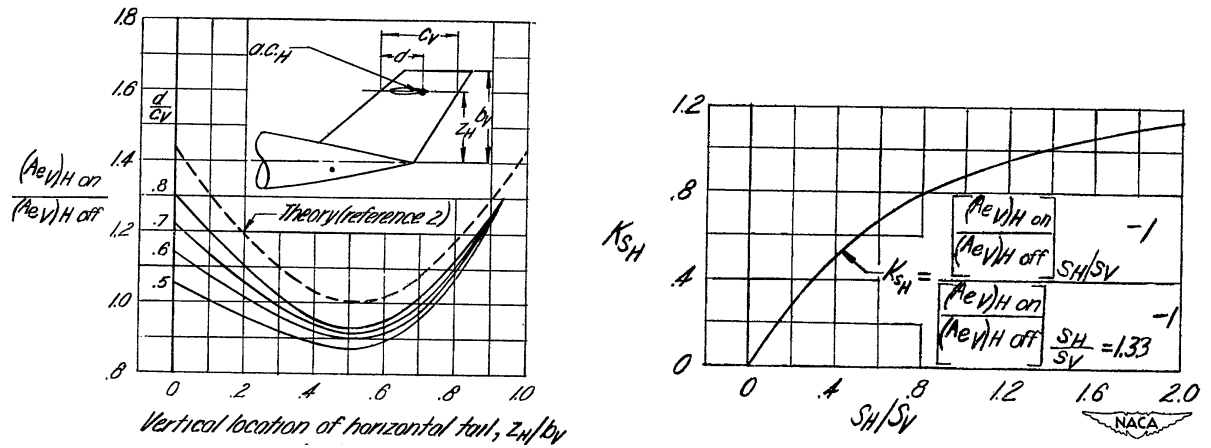
Figure 18: Horizontal tailplane position (left) and size (right) effects, according to NACA ref. [2].
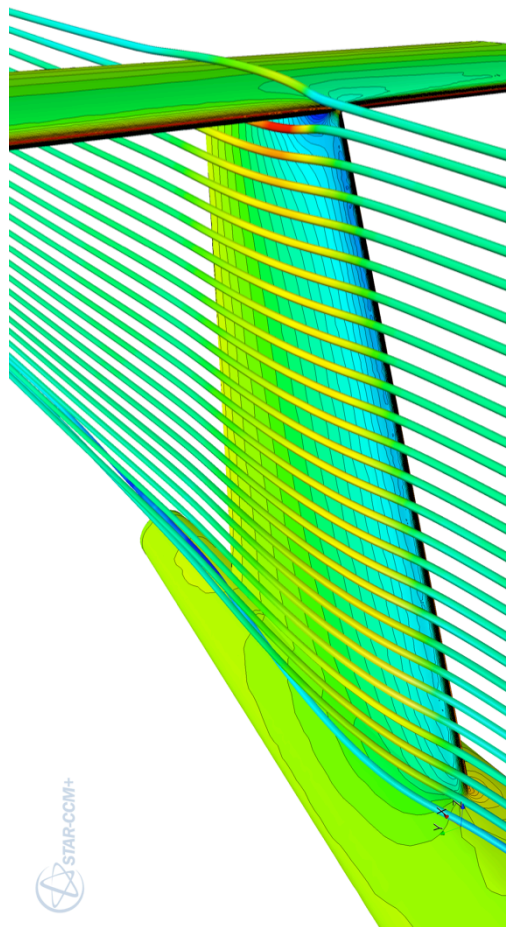

Figure 19: Streamlines and pressure contour on the fin-mounted (T-tail) configuration.

4 Conclusion

Text.

Acknowledgment

References

[1] Bamber, R. J., and House, R. O. (1939). Wind-tunnel investigation of effect of yaw on lateral-stability characteristics. II – Rectangular NACA 23012 wing with a circular fuselage and a fin. NACA.

[2] Brewer, J. D., and Lichtenstein, J. H. (1950). Effect of horizontal tail on low-speed static lateral stability characteristics of a model having 45° sweptback wing and tail surfaces. NACA.

[3] Eastmen, J. N., and Kenneth, W. E. (1935). Interferences of wing and fuselage from tests of 209 combinations in the NACA variable- density wind tunnel. NACA.

[4] Finck, R. D. (1978). USAF Stability and Control DATCOM. Wright-Patterson Air Force Base, Ohio: McDonnell Douglas Corporation.

[5] Gilbey, R. W. (1982). Contribution of fin to sideforce, yawing moment and rolling moment derivatives due to sideslip, $(Y_v)_F$, $(N_v)_F$, $(L_v)_F$, in the presence of body, wing and tailplane. ESDU.

[6] Nicolosi, F., Della Vecchia, P., and Corcione, S. (2012). Aerodynamic analysis and design of a twin engine commuter aircraft. ICAS.

[7] Perkins, C. D., and Hage, R. E. (1949). Airplane performance stability and control. Wiley.

[8] Queijo, M. J., and Wolhart, W. D. Experimental investigation of the effect of the vertical-tail size and length and of fuselage shape and length on the static lateral stability characteristics of a model with 45° sweptback wing and tail surfaces. 1950: NACA.

[9] Roskam, J. (1997). Airplane design part VI: preliminary calculation of aerodynamic, thrust and power characteristics. DAR Corporation.

[10] Weber, J., and Hawk, A. C. (1954). Theoretical load distributions on fin-body-tailplane arrangements in a side-wind. London, UK: Ministry of Supply.